The Race to X-ray Microbeam and Nanobeam Science

Gene E. Ice, John D. Budai, Judy W. L. Pang

X-ray microbeams are an emerging characterization tool with broad implications for science, ranging from materials structure and dynamics, to geophysics and environmental science, to biophysics and protein crystallography. We describe how submicrometer hard x-ray beams with the ability to penetrate tens to hundreds of micrometers into most materials and with the ability to determine local composition, chemistry, and (crystal) structure can characterize buried sample volumes and small samples in their natural or extreme environments. Beams less than 10 nanometers have already been demonstrated, and the practical limit for hard x-ray beam size, the limit to trace-element sensitivity, and the ultimate limitations associated with near-atomic structure determinations are the subject of ongoing research.

Around the world, scientists are racing to harness billion-dollar synchrotron facilities to generate and use ever-smaller hard x-ray microbeams and nanobeams (5 to 100 keV). This drive toward small x-ray beams is driven by three factors: (i) the fundamental interactions of x-rays with matter that allow for powerful characterization methods; (ii) the inhomogeneous nature of natural and human-made materials; and (iii) the emergence of ultrabrilliant synchrotron sources and efficient x-ray focusing optics. Indeed, the fundamental interactions of x-rays with matter make them effective probes for key materials characterization questions: What is the elemental composition? What is the local chemistry? What is the local crystal structure? What are the defects? For example, x-ray fluorescence analysis is for many samples the most sensitive nondestructive way to measure composition distributions, and x-ray fluorescence and absorption spectroscopies provide details about oxidation state, local coordination, and bond distances. X-ray scattering has also long been essential for determining crystal structures, and more than 18 Nobel Prizes have resulted from x-ray diffraction determinations of structures ranging from the double helix of DNA to the structure of fullerenes. Furthermore, the relatively weak interaction of x-rays with matter provides the opportunity to characterize samples nondestructively in the presence of air, water, or other environments with little or no sample preparation. The penetrating power of x-rays allows for studies in three dimensions (3D) and is a key factor in the ability of microbeams to affect virtually all scientific disciplines. What has been missing until recently is the ability to study small volumes.

Over the past three decades, specialized sources and instrumentation have evolved to meet the scientific challenges of x-ray micro/nanobeam experiments. Figure 1 illustrates the components of a generic synchrotron-based x-ray microprobe. Each component represents an active area of development. For example, as shown in Fig. 2A, x-ray source brilliance, the figure of merit for x-ray micro/nanobeams, continues to improve exponentially with a doubling time of 10 months. Similarly, achievable spot size (Fig. 2B) is also improving by a factor of 2 every 22 months. Indeed, it is now practical to make sensitive, quantitative measurements on volumes 10^3 to 10^5 times smaller than possible just a decade ago; scattering and fluorescence measurements on volume elements approaching 10^{-6} μm^3 are now possible. In addition to the ongoing revolution in source brilliance and focusing optics, specialized monochromators have been designed to maintain focal spot position during energy scans and to switch easily between monochromatic and broad-bandpass modes.

As the sample is moved under the beam, scattering or absorption processes are observed by various specialized x-ray detectors (Fig. 1). Elastic scattering in the form of single-crystal diffraction, powder diffraction, or coherent diffraction reveals atomic structure information and is measured by x-ray–sensitive area detectors. Inelastic scattering is observed by either energy or wavelength dispersive detectors to determine the elemental composition and chemistry. X-ray absorption spectroscopy can also be used to determine local chemistry. Powerful new methods can now depth-resolve sample volumes along the penetrating x-ray beam path.

How Are Submicrometer X-ray Beams and 3-D Spatial Resolution Achieved?

Although small x-ray beams can be produced by a number of methods, including capillary optics (*1*), crystal focusing (*2*), and waveguides (*3*),

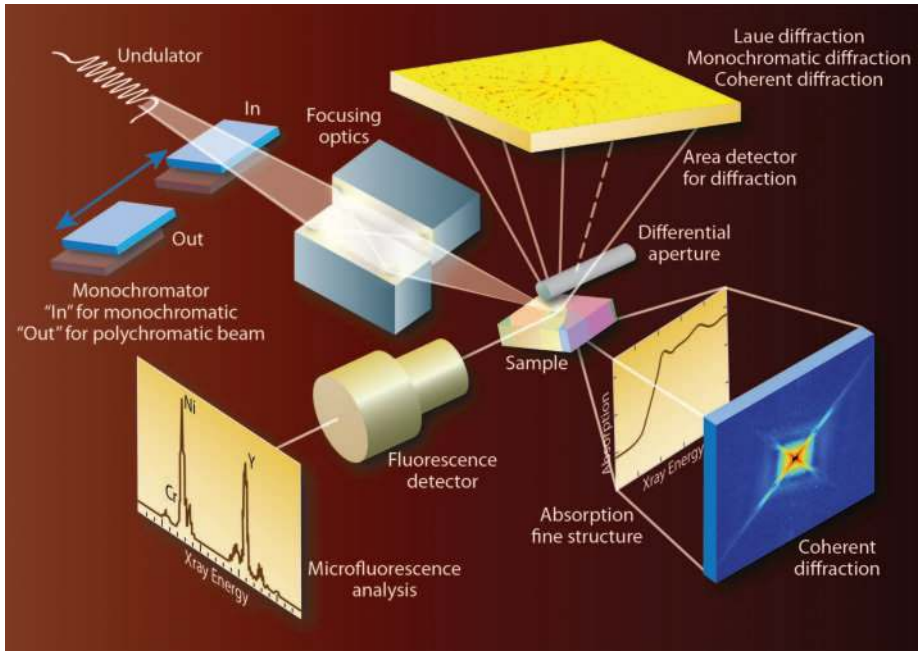

Fig. 1. A typical x-ray microprobe focuses x-rays from an ultrabrilliant undulator source to a submicrometer spot on a sample that is rastered under the beam. The x-rays can be used directly from the source for broad-bandpass applications or can be energy-selected by a special monochromator that preserves the beam focal spot position during energy scans. Scattering signals are observed by x-ray sensitive area detectors and/or energy-dispersive or wavelength-dispersive detectors that surround the sample. Possible signals include single-crystal diffraction, polycrystal diffraction, amorphous diffraction, coherent diffraction, absorption spectroscopy, and fluorescence. Differential aperture microscopy and other methods can be used to spatially resolve volume elements from along the penetrating path of the probe beam.

Oak Ridge National Laboratory, Oak Ridge, TN 37831–6132, USA.

*To whom correspondence should be addressed. E-mail: icege@ornl.gov

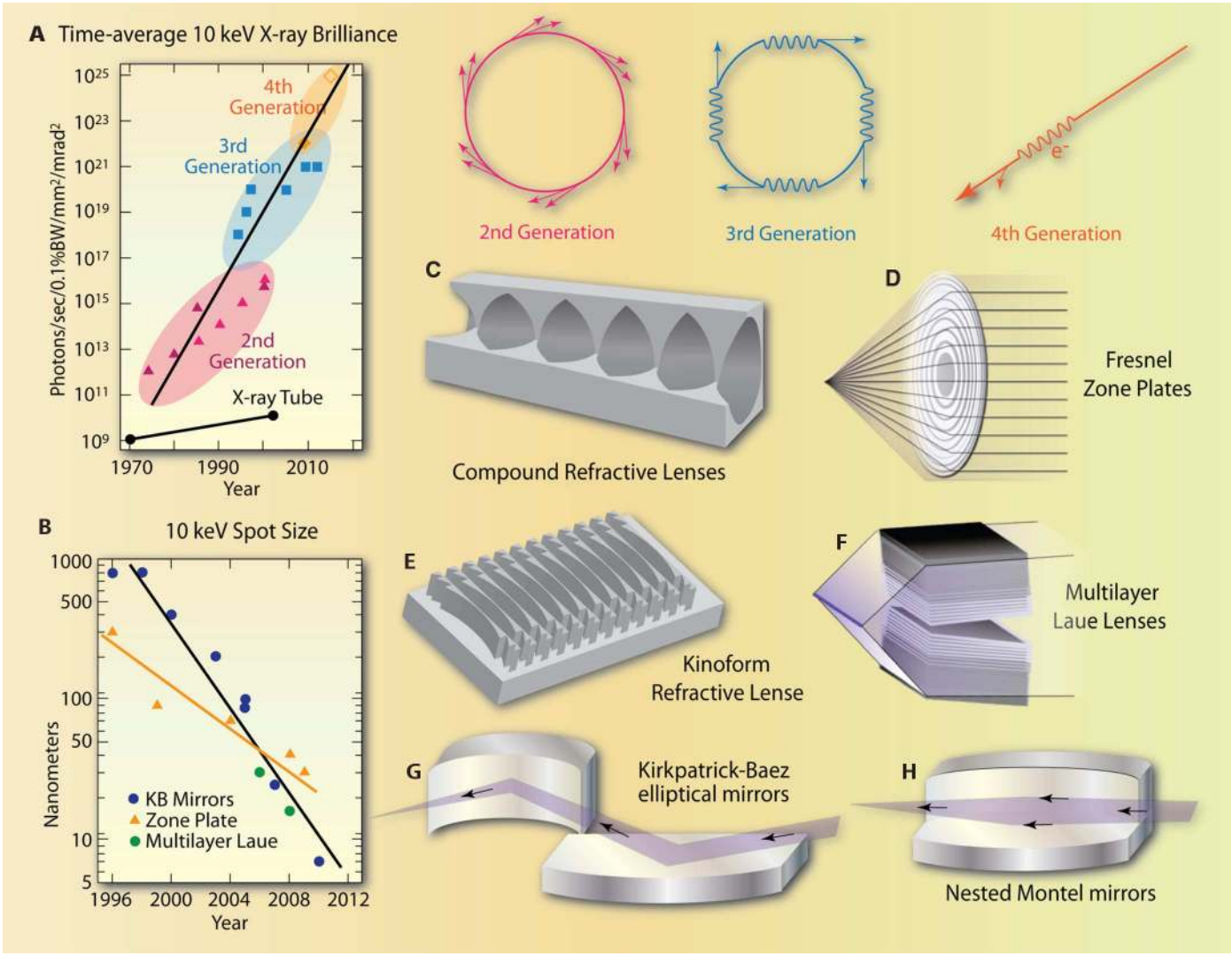

Fig. 2. (**A**) Synchrotron sources have evolved from early parasitic or first-generation to dedicated second-generation to third-generation sources using specialized magnetic configurations and, recently, to fourth-generation free-electron laser x-ray sources. (**B**) The achievable spot size for 10 keV x-rays has been revolutionized by major advances in precision fabrication of mirrors and zone plates and by new concepts. Beams as small as 7 nm have now been produced. (**C**) Compound refractive optics use multiple concave lenses to focus hard x-rays. (**D**) Zone plates are designed with different path lengths from each zone, so x-rays add constructively at the focus. (**E**) Kinoform lenses combine features of zone plates and compound refractive optics. (**F**) Multilayer Laue lenses use multilayer technologies to produce high-aspect-ratio 1D zone plates. (**G**) Kirkpatrick-Baez optics focus x-rays by sequential focusing with crossed elliptical x-ray mirrors. (**H**) Montel optics put elliptical mirrors side by side to focus larger divergences with a shorter focal length.

recent submicrometer developments have concentrated on three techniques: Kirkpatrick-Baez mirrors, zone plates, and compound refractive optics. During the past decade, these approaches have embraced wave-optical modeling and have developed fabrication controls needed to approach their ultimate diffraction limits. These approaches, with some important variants [see, for example, (*4*)], are illustrated in Fig. 2, C to H.

Refractive optics. Compound refractive x-ray lenses (Fig. 2C) have direct parallels to visible light focusing with refractive lenses but with special challenges because the index of refraction, n, for x-rays is nearly unity; the index of refraction of visible light in glass is $n \sim 1.5$, whereas for x-rays $n \sim 0.999997$. With $n \sim 1$, it difficult to bend x-rays with simple refractive lenses, and conventional wisdom held that refractive x-ray lenses were impractical. In the mid-1990s, however, it was realized that compound lenses composed of m discrete lenses multiply the small deflection of each lens m times (*5*). To reach nanometer-scale beams, sophisticated design and fabrication approaches are required that account for the evolving wavefield within the compound refractive lens (*6*). For example, the kinoform approach (Fig. 2E) combines elements of compound-refractive optics and zone-plate optics to reduce absorption and extend the achievable numerical aperture. Because the index of refraction of materials changes with x-ray wavelength (energy), compound refractive optics are inherently chromatic (i.e., dispersive). This limits their use for broad-bandpass focusing of microbeams but can enable novel instrumentation, including spectrometers. The smallest beams to date with compound refractive optics are ~50-nm diameter (*7*), but Schroer and Lengeler (*6*) and Evans-Lutterodt *et al.* (*8*) have demonstrated paths toward sub-10-nm beams.

Fresnel zone plates. X-ray focusing with zone plates (Fig. 2D) is another successful strategy for producing microbeams. Just as with optical zone plates, the path length from each zone is designed for constructive interference at the focus. Fresnel zone plates are straightforward to align, compact, and have a large field of view; as a consequence, they are particularly attractive for x-ray imaging applications, and zone plates with 30-nm resolution have been deployed for hard x-ray nanoprobes and for high-resolution x-ray imaging (*9*). Because

the focal length for constructive interference is proportional to x-ray wavelength, zone plates are chromatic, as is the case for refractive optics.

Multilayer Laue lenses. Multilayer Laue lenses (MLLs) (Fig. 2F) represent a promising planar variation on the zone-plate approach in which high-precision multilayer deposition techniques are used to produce relatively thick zone plates consisting of thousands of layers and with very thin outer zones that enable high resolution. Because a single MLL produces a line focus, crossed pairs are needed for point microbeams. In addition, improved focusing is achieved by uniformly or variably tilted MLLs. These high-aspect devices have already demonstrated line-focusing to 16 nm (*10*), and they are projected to reach single nanometer resolution.

Mirror optics. The oldest method for microfocusing x-rays is with mirror optics (Fig. 2, G and H). X-ray mirrors can be either single-layer total-external-reflection mirrors, which reflect wide-bandpass beams at very low (a few milliradian) glancing angles, or multilayer mirrors that reflect 10 to 0.1% energy bandpasses at larger but still glancing angles. Most mirrors for micro/nanofocusing are elliptical Kirkpatrick-Baez mirrors (Fig. 2G) as pioneered by Kirkpatrick and Baez in the 1940s for an x-ray microscope. Kirkpatrick-Baez mirror focusing has recently achieved a 7-nm focused x-ray beam at 20 keV by combining adaptive optics, multilayer mirrors, and ultrasmooth, near-atomic polishing methods (*11*). Because mirror optics are inherently achromatic, they are attractive for wide-bandpass applications such as fluorescence analysis, Laue diffraction measurements, and energy scanning techniques. Other variants of Kirkpatrick-Baez optics, such as nested Montel mirrors (Fig. 2H), offer important advantages in terms of compactness and improved diffraction limit.

Three-dimensional spatial resolution. Small x-ray beams can spatially resolve in 2D, but average over extended volumes as they penetrate into bulk samples. Two approaches have emerged for resolution in 3D: tomographic methods (*12*, *13*) and confocal or x-ray–triangulation methods (*14*–*16*). X-ray tomographic methods are an extension of conventional (medical) computer-aided tomography in which high-resolution x-ray detectors are used to achieve submicrometer 3D maps of sample density and/or chemistry. Three-dimensional spatial resolution of ~30 nm has been demonstrated (*17*), and phase-contrast techniques can be used to image low–atomic number structures. Although tomography does not typically use microfocused beams, fluorescence tomography is an ultrasensitive method for determining trace-element distributions, capable of detecting concentrations below parts per million (ppm) levels (*18*), that requires doubly-focused microbeams. Further description of the technique and an example of an experimental tomographic reconstruction of trace-element distributions in SiC shells of advanced nuclear fuel (*19*) is provided in the supporting online material (SOM) (fig. S1). Three-dimensional composition maps can also be made using confocal or triangulation methods (*20*). Here, the volume element along the beam path is isolated by a slit placed close to the sample or by an x-ray lens with its axis normal to the beam direction. These methods are particularly well suited to layered structures and are described in the SOM fig. S2.

For diffraction measurements, differential aperture microscopy is a triangulation method that resolves submicrometer volumes along the penetrating path of a doubly-focused x-ray microbeam (*14*, *21*). In this technique, an absorbing wire is passed through a diffraction pattern at a height just above the surface of the sample (Fig. 1). The wire acts as an absorbing knife-edge. Occluded intensity at each pixel on the detector can be traced back to its origin inside the sample by triangulation. This method provides submicrometer spatial resolution in 3D without the need for destructive sample sectioning or sample rotations. Movie 1 illustrates the method, and movie 2 shows a depth-resolved diffraction pattern. Differential aperture microscopy for elemental mapping will become possible with low-noise energy-resolving area detectors.

Using a different approach, 3D x-ray diffraction microscopy is another 3D triangulation method that relies on singly-focused (planar) high-energy (50 to 100 keV) monochromatic x-ray beams (*16*). The sample is rotated to collect multiple Bragg reflections, and grain positions and shapes are determined by triangulation. This method is ideal for rapidly and nondestructively mapping millions of volume elements and, hence, is particularly well-suited for measurements of evolving 3D crystal structures (figs. S4 and S5 show the schematic setup and the grain orientation map of a Ni sample determined using this approach). The present spatial resolution of a few micrometers is projected to reach submicrometers as tomographic methods are combined with submicrometer-resolution x-ray area detectors.

What Do X-ray Microbeams Tell Us About Local Composition and Chemistry?

The potential of x-ray microbeams to map elemental composition and detect trace elements in materials was recognized by early synchrotron scientists. For example, a 1977 x-ray microfluorescence search for superheavy elements by Sparks and co-workers was a pivotal synchrotron experiment (*22*). This experiment focused 37 keV x-rays to what was then an exotically small ~250-μm spot. The trace-element measurements (~50 ppm) refuted a proton microprobe report of primordial superheavy elements (atomic numbers 114 to 127) in small rock inclusions.

Driven by the characterization opportunities afforded by micro–x-ray fluorescence spectroscopy (μXFS) and micro–x-ray absorption near-edge spectroscopy (μXANES), these methods have evolved into sophisticated tools for mapping elemental distributions and chemistry. For example, to understand how cells segregate heavy metals under normal and toxic conditions, Matsuyama *et al*. (*23*) used μXFS to investigate mitochondria in single cells labeled with 5-nm colloidal Au particles. Using a Kirkpatrick-Baez mirror focusing system at the SPring-8 synchrotron, trace-element distributions of P, S, Cl, Ca, Fe, Cu, Zn, and Au were mapped with less than 100-nm resolution. Spatial resolution of 30 nm is now available, which opens important opportunities for understanding how trace elements are distributed in healthy and diseased cells (Fig. 3A).

The companion tool, μXANES, represents a quantitative technique for spatial mapping of the oxidation states of elements. This capability reveals chemical variations needed to understand how biological and chemical processes proceed at the microstructural or intracellular level. Although this information is vital in almost all areas of materials science, it is particularly intriguing to speculate how μXANES could help improve microbiological techniques for treating diseases. For example, several groups are using μXFS and μXANES to locate and explore the role of transition metals in neurodegenerative disorders such as Alzheimer's and Parkinson's diseases (*24*, *25*). Elevated concentrations and oxidation reactions involving elements such as Fe, Cu, and Zn are associated with later stages of these diseases. However, a suggestion that the metals cause oxidative stress that leads to the death of nerve cells remains only a hypothesis. By examining particular chemical mechanisms participating in the degeneration processes inside individual neurons, researchers hope to guide techniques aimed at early diagnosis or cures.

Due to the broad need for chemical mapping, microspectroscopies, including μXFS, and μXANES, are increasingly being used by researchers from scientific fields not typically familiar with synchrotron facilities, including astrophysics, archaeology, paleontology, and art history. For example, recent studies of interstellar particles collected by the NASA Stardust spacecraft identified inhomogeneous distributions of several elements with very high 3D spatial resolution of 200 nm (*26*). Another recent study measured the trace-element abundances in presolar SiC grains found inside a primitive meteorite (*27*). These micrometer-sized stardust grains are believed to originate from the outflow of stellar material that predates the solar system, and the 600-nm resolution μXFS analysis suggested that they condensed from stars depleted in Zr but not in Nb. The authors speculate that the Zr deficiency could have been caused by ZrC condensation coupled with eviction by outward radiation pressure. More broadly, these measurements demonstrate how the ability to quantify particular primordial nuclear and chemical processes can enhance our understanding of cosmological forces billions of years ago.

What Do X-ray Microbeams Tell Us About Microstructure and Evolution Inside Materials?

X-ray micro- and nanodiffraction probes can now map how structures change from point to point

inside samples. Because almost all technologically important materials and all biological materials are structurally inhomogeneous on multiple length scales, micro/nano probes are certain to play increasingly important roles as science transitions from mean-field ensemble averages to an emphasis on local environments and local deviations from average behavior.

There are numerous materials-science issues that require local structure information. With processes such as deformation, grain growth, and fracture, important questions include the following: What is the influence of free surfaces, interfaces, and grain boundaries on deformation? What are the underlying drivers for the aggregation and evolution of dislocations into self-organized 3D patterns surrounding "cell structures" in deformed ductile metals? What factors control the thermal growth of grains, and why does one grain grow at the expense of its neighbor? How do materials shield fracture to arrest crack propagation in ductile materials. These are grand-challenge questions of materials science that hold the keys to understanding how real materials behave over hierarchical length scales and that impact our ability to predict materials behavior.

Consider the ubiquitous role of grain sizes and morphology in controlling physical properties. Many technologically important materials, including next-generation solar cells, turbine blades, sintered ceramics, and high-strength alloys, are carefully processed to control grain microstructures. Despite advances in computer modeling, at present we cannot accurately predict how grain sizes or orientations (texture) will evolve during thermal grain growth, even for simple single-component systems.

Recent advances in x-ray microdiffraction have enabled detailed nondestructive measurements of 3D grain growth inside polycrystal samples (*28*–*30*). For example, submicrometer-resolution 3D maps after successive thermal annealing steps were used to detail the migration of every grain boundary viewed inside a hot-rolled polycrystalline Al sample (Fig. 3B). Moreover, the high spatial and angular resolution (~0.01°) of x-ray microdiffraction measurements (*29*) makes it possible to map the local line defects (dislocation) density inside individual grains. The distribution of these intragranular defects and their stored energy are known to strongly effect recrystallization and grain growth. Spatially resolved measurements such as these are essential to quantitatively test the underlying mechanisms used in large-scale computer models.

In another growth example of relevance to electronics reliability (Fig. 3C), the ability to map both grain orientation and local elastic stress has been used to directly test theories of mesoscale formation and growth of Sn whiskers in electronic devices (*31*). In these experiments, the residual strain distribution near the root of fresh Sn whiskers was characterized to critically examine theories of spontaneous Sn whisker growth, a reliability issue for Pb-free solders. The measured strains supported a growth model based on strain gradients induced by intermetallic phases that develop at the Cu/Sn interface and grow into the grain boundaries.

In addition to thermal treatments, mechanical deformation remains a cornerstone of materials processing and a key element in materials failure. A long-standing question in this field is "what is surface versus bulk?" For example, atomic force microscopy morphology measurements have found that surface profiles of deformed single crystals show scale invariance from nanometers to millimeters (*32*). To understand 3D deformation, depth-resolved x-ray microdiffraction measured the local rotations in deformed Cu single crystals with micrometer resolution over hundreds of micrometers parallel to the surface and tens of micrometers perpendicular to the surface (*33*). The results reveal that there is a surface region with a universal deformation behavior, as previously observed, but that deformation changes a few tens of micrometers below the surface in a transition zone that depends on the crystal orientation. This process is conceptually understood in terms of multiple slip-system lock-up. However, no quantitative theoretical model has yet been developed, and collaborative microdiffraction and theoretical work will likely be critical for developing predictive models of how surfaces and interfaces influence 3D deformation. More details are provided in the SOM of how to resolve local deformation in intercrystalline regions in a deformed polycrystal (fig. S3 and movie 3).

Local microstructure impacts physical properties beyond mechanical behavior. For exam-

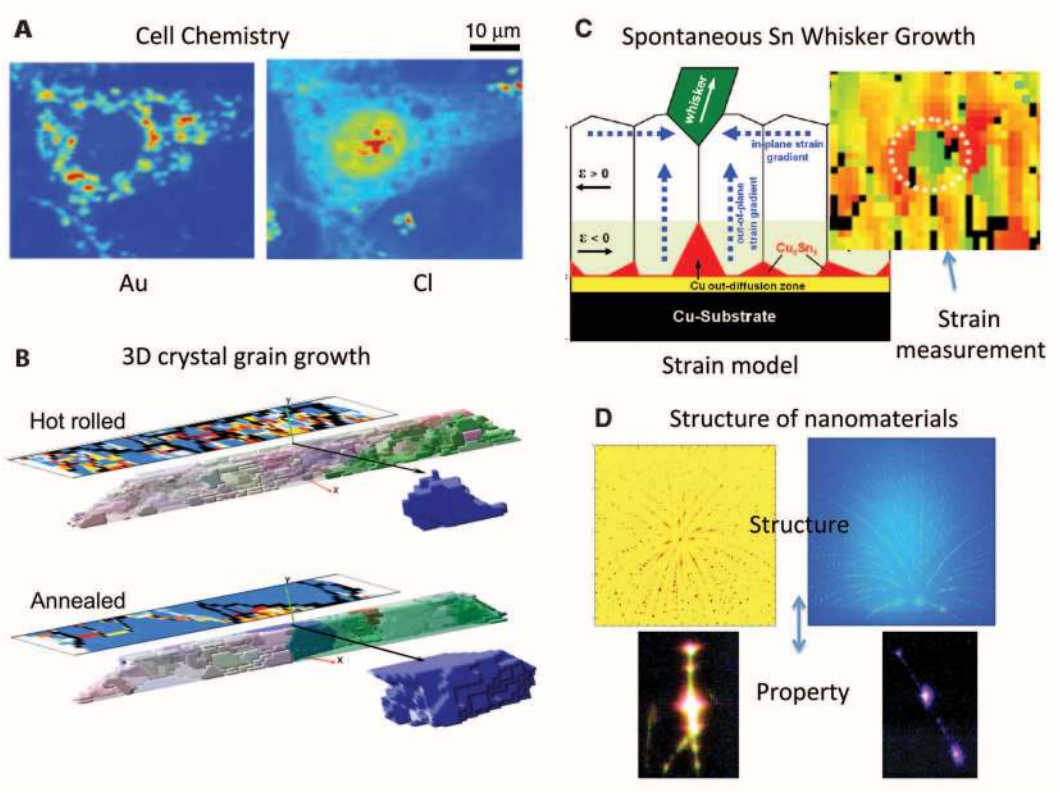

Fig. 3. (**A**) Distribution of trace elements by 100-nm μXFS in a single cell with Au-labeled mitochondria (*23*). (**B**) 3D grain maps detail the migration of every boundary viewed inside a 3D polycrystalline sample after thermal annealing (*29*). Single grains are removed from the 3D maps to illustrate how a particular grain has evolved inside the ~10 by 10 by 100 μm^3 volume. In addition, the planes to the left of each map are color-coded horizontal slices showing the measured local defect densities. As the grains grow, internal defects are dramatically reduced. (**C**) Model for spontaneous Sn whisker growth from a Cu substrate and direct experimental measurement of proposed strain gradients near the whisker root (*31*). (**D**) Crystal diffraction patterns for two europium aluminate nanorods showing distinct photoluminescence properties associated with distinct lattice structures.

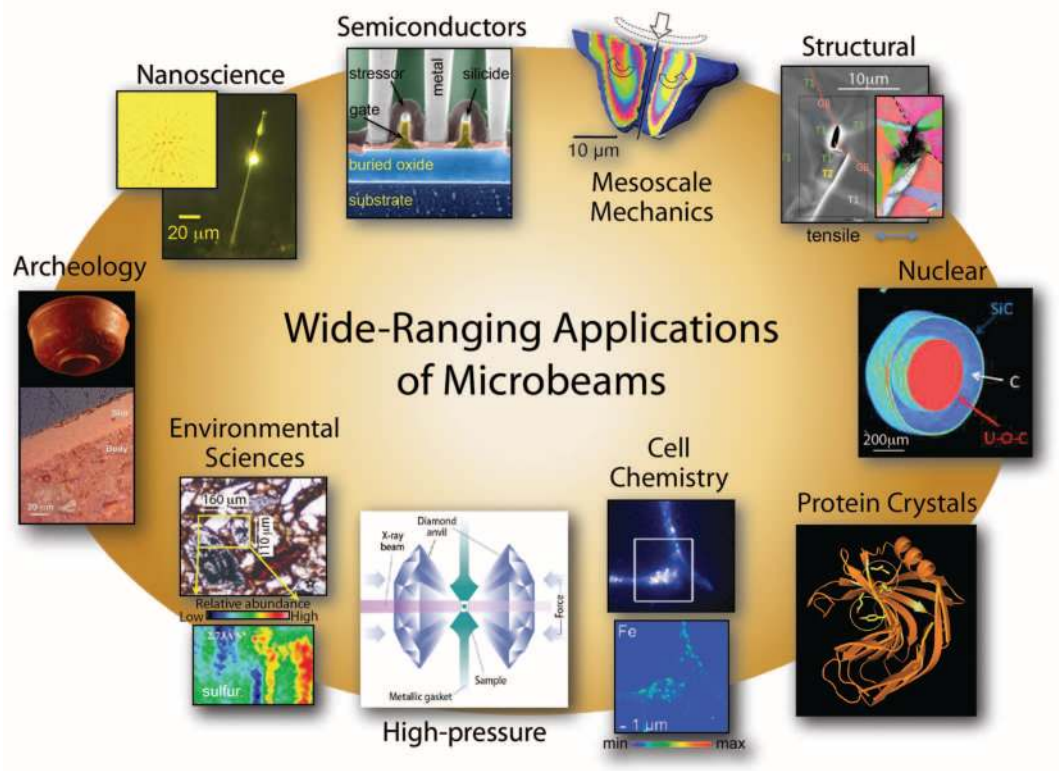

Fig. 4. Wide-ranging applications of microbeams. (Clockwise from upper left) The nanoscience μLaue diffraction pattern and image showing strong yellow microbeam-induced photoluminescence were obtained from a SrEuAlO nanowire grown by Z. W. Pan (University of Georgia). In semiconductor devices such as the IBM POWER6 processor (courtesy of IBM Microelectronics), microbeams have been used to study carrier mobility enhancement due to local strain engineering (*50*). The mesoscale mechanics image shows a false-color map of the measured rotations around a microindented Cu single crystal, which can be used to test theoretical models (courtesy of B. C. Larson, ORNL). The structural example shows how local heterogeneous strains interact with grain boundaries to produce a microcrack in Ti (*53*). The nuclear example shows tomographic imaging of C and SiC layers surrounding the U–O–C core of a submillimeter tristructural-isotropic fuel particle (courtesy of E. Specht, ORNL). The protein crystal image shows a structure in xylanase II that has been determined to a resolution of 0.15 nm (*38*). The cell chemistry example uses nanofluorescence to map the iron distribution within individual dopamine neurovesicles (*54*). The high-pressure image shows a typical diamond-anvil geometry enabling pressures of up to 300 GPa for synchrotron diffraction measurements (*42*). The environmental sciences image shows the sulfur trace-element distribution within different mineralogical phases for a sample from a former mining site (*49*). The archaeology example shows Roman-period terra sigillata pottery and illustrates how microstructural analysis can reveal the materials and processing steps used by ancient craftsmen (*52*).

ple, the emergence of remarkable electronic properties such as colossal magnetoresistance in strongly correlated electron materials is believed to be coupled with local nanoscale to mesoscale structural domains and strains (*34*). X-ray micro/nanobeams can now connect local structure to emergent electronic or optical properties. For example, spatially resolved measurements on nanostructured materials can be used to identify local phases or internal domain boundaries and thus help to understand the structural origins of properties such as the photoluminescence spectra from novel nanowhiskers (Fig. 3D).

In another recent example, several research groups have initiated microdiffraction studies of the structural-electronic relationship in a classic metal-insulator system, vanadium dioxide (*35*–*37*). VO_2 exhibits a coupled phase and electronic [metal insulator transition (MIT)] change at 67°C. Understanding how electron-electron (Mott MIT) and electron-phonon (Peierls MIT) correlations interact to drive this MIT have remained controversial for decades. Recent nanoprobe work imaged both the structural and electronic order parameters as a VO_2 film was thermally cycled (*37*). The authors observed a dichotomy in behaviors, with a continuous monotonic progression of growing electronic domains but nonmonotonic local structural switching. These contrasting observations suggest that the electronic and structural transitions are coupled by complex and as yet unexplained nanoscale mechanisms.

How Will Focused X-ray Microbeams Enable Studies of Small Crystals and Unique Sample Environments?

X-ray microbeams provide important opportunities in situations where measurements can only be obtained from a small sample or a small volume. For example, it is often difficult to grow large protein crystals, and extreme environments (e.g., high pressures) are often limited to small volumes. In each case, small probes allow for advanced characterization that would otherwise be difficult or impossible.

For protein crystallography, microbeams offer transformative advantages: (i) they provide the best signal-to-noise ratio for small crystals; (ii) they can be used to probe undamaged volumes during sample rotations in even small crystals; (iii) if divergence is not too great, the small beam size makes for very sharp diffraction spots; (iv) they can be used to find volumes of low mosaic spread in large crystals with nonuniform structural order; and (v) small size may reduce sample damage rates by photoelectron escape (*38*).

For example, Sawaya *et al*. (*39*) used microbeams to determine the atomic structures of 45 fibril-forming proteins that form both fibrils and microcrystals with resolution between 0.08 and 0.2 nm. This work, which depended on the ability to efficiently study very small microcrystals, found that fibrils associated with various disease states had similar atomic structures. In other studies by Rasmussen *et al*. (*40*) and Rosenbaum *et al*. (*41*), the structure of a seven-transmembrane helix, G protein–coupled receptor was determined through the use of a small 7-μm beam and an associated search strategy to find a volume of high crystallographic order.

In high-pressure science, the smaller the sample, the higher the pressure that can be achieved. Diamond anvil cells can achieve the highest pressures of any static loaded cell but can only work on samples tens to hundreds of micrometers in size. As a result, small x-ray beams with the ability to penetrate through the gasket or anvil material are essential. Currently, pressures of up to 300 GPa can be achieved in cells designed for microbeam synchrotron studies. Researchers from the High Pressure Synergetic Consortium at the Advanced Photon Source (APS) recently discovered that Y_2O_3, a common material used in industrial coatings, transforms differently under pressure as a function of particle size. Using pressures over 30 GPa, they found that phase stabilities for cubic, hexagonal, and amorphous structures were very different for nanoparticles than for bulk materials, thus demonstrating how particle size can affect properties under extreme conditions (*42*).

Nuclear materials are another example where x-ray microbeams can provide new information in small samples. Nuclear materials not only are

notoriously heterogeneous but also can be dangerous to handle in normal engineering sizes. Very small samples, however, can be safely handled with orders of magnitude of lower activity. For example, Specht and co-workers (*43*) have used an x-ray microbeam to study the diffuse scattering from defects in ion-irradiated grains in a thin Fe film. This experiment demonstrates the ability to treat individual grains like single crystals and the ability to make difficult measurements on very small sample volumes.

Outlook

The practical limit for x-ray beam size remains an unanswered question. Although past focusing systems were constrained mainly by the perfection of the fabricated focusing structures, recent focusing optics have become more fundamentally constrained by the diffraction limit. This constraint imposes the need to increase the numerical aperture of focusing optics.

Mirror optics currently hold the record for the smallest focused x-ray beams (7 nm), but the theoretical limits for all focusing methods continue to improve with more advanced strategies. For example, the APS upgrade plan calls for a goal of <5 nm with x-rays above 25 keV using MLL optics. In the case of both MLLs lenses and compound refractive optics, there are major challenges associated with the wavefield evolution in the optics. For compound refractive optics, this evolution can be handled by adapting the refractive structure along the length of the compound lens. In addition, kinoform designs can be used to decrease beam absorption for higher efficiency compound refractive lenses. For MLLs, the wavefield evolution inside the device can be mitigated by tilting the lens, introducing a wedged aspect ratio to the layers, or by introducing curvature through the thickness of the lens.

With mirror optics, even more complicated optical strategies can be used to reach smaller beams. Wolter optics that focus from paired surfaces of revolution offer the potential for a larger field of view and a factor of 3 to 4 smaller diffraction limit. Although there is not a clear path toward making sufficiently perfect Wolter optics to approach the current performance of Kirkpatrick-Baez mirrors, other multiple mirror strategies appear practical in the near future if more complicated focal structures with multiple ultrasmall peaks are acceptable (*44*).

As x-ray beams become ever smaller, some important capabilities appear to be within reach. For example, a straightforward calculation of trace-element sensitivity indicates that there should be sufficient signal from a 1-nm probe to detect a single high-Z atom in a low-Z matrix (*45*). This calculation does not include loss of sensitivity due to sample background or the change in properties due to sample damage but raises the possibility of monitoring the influence of single atoms on device behavior.

Another grand-challenge goal is atomic spatial resolution. One possible means to achieve this goal is through coherent diffraction imaging. Coherent diffraction imaging can exploit diffraction-limited microbeams to achieve spatial resolution far below the probe size, and recent experiments have demonstrated the importance of microfocused x-ray beams for achieving the highest spatial resolution (*46*, *47*). Microfocusing increases the flux density on the sample at the expense of field of view. High flux density is required to measure the weak coherent diffraction tails that ultimately sets the coherent diffraction spatial resolution. Recent measurements using nearly diffraction-limited Kirkpatrick-Baez mirrors have now demonstrated spatial resolution of 2 nm (*48*). With projected increases of x-ray brilliance of four orders of magnitude in future synchrotrons, spatial resolution approaching 0.2 nm should be possible, assuming that samples are not damaged by the more intense beams.

Of course, as microbeam spatial resolution improves, the kind of science that is possible has begun to overlap the domain of electron microscopy methods, including electron holography, transmission electron microscopy, and quantitative scanning electron microscopy. The main advantage of x-rays over more readily available electron methods is their ability to probe samples buried in hostile environments, underwater, and/or through layered structures, and the tremendous quantitative sensitivity of x-rays to trace elements and structure. When combined, the emerging suite of electron and x-ray structural probes will enable characterization over all hierarchical length scales ranging from atomic to macroscopic.

Finally, we note that, since structural inhomogeneities affect performance in practically all materials, both natural and manmade, microbeam structural characterization will eventually extend to many areas of science not covered explicitly in this review. As highlighted in Fig. 4, geologists and environmental scientists need 3D maps to reveal mineral interactions as toxic elements leach from mines (*49*); semiconductor devices increasingly rely on enhanced carrier mobilities through local strain engineering in nanoscale features (*50*); many biological architectures, including bones and teeth, are highly organized hierarchical composite structures (*51*); and even archaeologists and art historians need nondestructive characterization to understand material processes used by past civilizations (*52*). Clearly, x-ray micro/nanobeam methods are poised to affect both a broad range of science and long-standing grand-challenge issues.

References and Notes

1. R. A. Barrea, R. Huang, S. Cornaby, D. H. Bilderback, T. C. Irving, *J. Synchrotron Radiat.* **16**, 76 (2009).
2. C. Schulze, U. Lienert, M. Hanfland, M. Lorenzen, F. Zontone, *J. Synchrotron Radiat.* **5**, 77 (1998).
3. W. Jark *et al.*, *Appl. Phys. Lett.* **78**, 1192 (2001).
4. www.x-ray-optics.com
5. A. Snigirev, V. Kohn, I. Snigireva, B. Lengeler, *Nature* **384**, 49 (1996).
6. C. G. Schroer, B. Lengeler, *Phys. Rev. Lett.* **94**, 054802 (2005).
7. C. G. Schroer *et al.*, *Appl. Phys. Lett.* **87**, 124103 (2005).
8. K. Evans-Lutterodt *et al.*, *Phys. Rev. Lett.* **99**, 134801 (2007).
9. www.xradia.com/products/xray-optics/index.php
10. C. Liu *et al.*, in *SRI 2009: The 10th International Conference on Synchrotron Radiation Instrumentation*, R. Garrett *et al.*, Eds. (2010), vol. 1234, pp. 47–50.
11. H. Mimura *et al.*, *Nat. Phys.* **6**, 122 (2010).
12. A. Sakdinawat, D. Attwood, *Nat. Photonics* **4**, 840 (2010).
13. P. Bleuet *et al.*, *Trends Anal. Chem.* **29**, 518 (2010).
14. B. C. Larson, W. Yang, G. E. Ice, J. D. Budai, J. Z. Tischler, *Nature* **415**, 887 (2002).
15. H. F. Poulsen *et al.*, *J. Appl. Cryst.* **34**, 751 (2001).
16. H. F. Poulsen, *Three-Dimensional X-Ray Diffraction Microscopy: Mapping Polycrystals and Their Dynamics* (Springer-Verlag, Berlin, 2004).
17. J. C. Andrews *et al.*, *Microsc. Microanal.* **16**, 327 (2010).
18. I. Letard *et al.*, *Rev. Sci. Instrum.* **77**, 063705 (2006).
19. M. Naghedolfeizi *et al.*, *J. Nucl. Mater.* **312**, 146 (2003).
20. L. Vincze *et al.*, *Anal. Chem.* **76**, 6786 (2004).
21. B. C. Larson, J. Z. Tischler, A. El-Azab, W. J. Liu, *J. Eng. Mater. Tech. Trans. ASME* **130**, 021024 (2008).
22. C. J. Sparks, S. Raman, E. Ricci, R. V. Gentry, M. O. Krause, *Phys. Rev. Lett.* **40**, 507 (1978).
23. S. Matsuyama *et al.*, *X-Ray Spectrom.* **38**, 89 (2009).
24. J. Chwiej *et al.*, *J. Trace Elem. Med. Biol.* **22**, 183 (2008).
25. J. F. Collingwood *et al.*, *J. Alzheimers Dis.* **7**, 267 (2005).
26. G. Silversmit *et al.*, *Anal. Chem.* **81**, 6107 (2009).
27. Y. Kashiv *et al.*, *Astrophys. J.* **713**, 212 (2010).
28. S. Schmidt *et al.*, *Science* **305**, 229 (2004).
29. J. D. Budai *et al.*, *Mater. Sci. Forum* **467–470**, 1373 (2004).
30. U. Lienert *et al.*, in *THERMEC' 2006, Pts. 1–5*, T. Chandra, K. Tsuzaki, M. Militzer, C. Ravindran, Eds. (Trans Tech Publications, Stafa-Zuerich, Switzerland, 2007), vols. 539–543, pp. 2353–2358.
31. M. Sobiech *et al.*, *Appl. Phys. Lett.* **94**, 221901 (2009).
32. M. Zaiser, F. M. Grasset, V. Koutsos, E. C. Aifantis, *Phys. Rev. Lett.* **93**, 195507 (2004).
33. J. W. L. Pang, G. E. Ice, W. J. Liu, *Mater. Sci. Eng. A* **528**, 28 (2010).
34. K. H. Ahn, T. Lookman, A. R. Bishop, *Nature* **428**, 401 (2004).
35. A. Tselev *et al.*, *Nano Lett.* **10**, 2003 (2010).
36. J. Cao *et al.*, *Nano Lett.* **10**, 2667 (2010).
37. M. M. Qazilbash *et al.*, *Phys. Rev. B* **83**, 165108 (2011).
38. R. Moukhametzianov *et al.*, *Acta Crystallogr. D Biol. Crystallogr.* **64**, 158 (2008).
39. M. R. Sawaya *et al.*, *Nature* **447**, 453 (2007).
40. S. G. F. Rasmussen *et al.*, *Nature* **450**, 383 (2007).
41. D. M. Rosenbaum *et al.*, *Science* **318**, 1266 (2007).
42. L. Wang *et al.*, *Phys. Rev. Lett.* **105**, 095701 (2010).
43. E. D. Specht, F. J. Walker, W. J. Liu, *J. Synchrotron Radiat.* **17**, 250 (2010).
44. G. E. Ice *et al.*, *Mater. Sci. Eng. A* **524**, 3 (2009).
45. D. H. Bilderback, R. Huang, in *Synchrotron Radiation Instrumentation*, T. Warwick *et al.*, Eds. (2004), vol. 705, pp. 1271–1274.
46. C. G. Schroer *et al.*, *Phys. Rev. Lett.* **101**, 090801 (2008).
47. P. Thibault *et al.*, *Science* **321**, 379 (2008).
48. Y. Takahashi *et al.*, *Phys. Rev. B* **82**, 214102 (2010).
49. A. Courtin-Nomade, H. Bril, J. M. Beny, M. Kunz, N. Tamura, *Am. Mineral.* **95**, 582 (2010).
50. C. E. Murray *et al.*, *Appl. Phys. Lett.* **94**, 063502 (2009).
51. C. E. Killian *et al.*, *J. Am. Chem. Soc.* **131**, 18404 (2009).
52. Y. Leon *et al.*, *Appl. Phys. A, Mater. Sci. Process.* **99**, 419 (2010).
53. L. Wang *et al.*, *Metall. Mater. Trans. A, Phys. Metall. Mater. Sci.* **42**, 626 (2011).
54. R. Ortega, P. Cloetens, G. Devès, A. Carmona, S. Bohic, *PLoS ONE* **2**, e925 (2007).

Acknowledgments: Research sponsored by the U.S. Department of Energy (DOE), Office of Basic Energy Sciences, Materials Sciences and Engineering Division under contract DE-AC05-00OR22725 with UT-Battelle, LLC. Research included use of beamline 34-ID at the Advanced Photon Source, a U.S. DOE Office of Science User Facility.

Supporting Online Material

www.sciencemag.org/cgi/content/full/334/6060/1234/DC1
SOM Text
Figs. S1 to S5
Movies S1 to S3
References

10.1126/science.1202366